


Many-body localization transition from flat-band fine tuningCarlo Danieli¹,² Alexei Andreanov^{2,3} and Sergej Flach^{2,3}¹Max Planck Institute for the Physics of Complex Systems, Dresden D-01187, Germany²Center for Theoretical Physics of Complex Systems, Institute for Basic Science (IBS), Daejeon 34126, Korea³Basic Science Program, Korea University of Science and Technology (UST), Daejeon 34113, Korea (Received 22 April 2021; revised 11 January 2022; accepted 11 January 2022; published 28 January 2022)

Translationally invariant flatband Hamiltonians with interactions lead to a many-body localization transition. Our models are obtained from single-particle lattices hosting a mix of flat and dispersive bands, and equipped with fine-tuned two-body interactions. Fine-tuning of the interaction results in an extensive set of local conserved charges and a fragmentation of the Hilbert space into irreducible sectors. In each sector, the conserved charges originate from the flatband and act as an effective disorder inducing a transition between ergodic and localized phases upon variation of the interaction strength. Such fine-tuning is possible in arbitrary lattice dimensions and for any many-body statistics. We present computational evidence for this transition with spinless fermions.

DOI: [10.1103/PhysRevB.105.L041113](https://doi.org/10.1103/PhysRevB.105.L041113)

Introduction — The celebrated Anderson localization [1] with additional interactions leads to a novel phase of matter dubbed many-body localization (MBL). Efforts to understand this phase generated an impressive body of work devoted to the study of non-equilibrium quantum many-body systems. Following the first pioneering papers [2–6], a large number of MBL-related theoretical and experimental studies focused on the interplay of disorder and interaction—as summarized in Refs. [7,8]. Interestingly, a variety of diverse interacting systems were reported to enter MBL phases even in the absence of disorder [9–12], from networks of Josephson junctions [13] to Wannier-Stark many-body localization [14–16]. This opened an active research quest dedicated to disorder-free MBL. Ergodicity breaking in disorder-free setups can appear due to the splitting of the Hilbert space into exponentially large number of disconnected parts. It is induced by the presence of an extensive number of local conserved quantities. Discussions relate to lattice models endorsing spin-duality relations [17–19] or gauge invariance [20], a two-dimensional quantum-link network [21], and a two-leg compass ladder [22]. Examples of such splitting have been also found in setups without any apparent extensive number of conserved quantities, e.g., in systems conserving dipole moments [23] or domain-wall numbers [24]. While first realizations of this phenomenon have been recently emerging [25], the above references utilize rather abstract models whose applicability to experimental realizations might be far from trivial.

We use translationally invariant short-range flatband Hamiltonian networks. Geometric frustration in these fine-

tuned systems results in a mix of dispersionless (flat) and dispersive Bloch bands. A hallmark is the existence of compact localized (eigen)states (CLS) spanned over a finite number U of unit cells. Flatband lattices and CLS have been extensively studied over the last decades [26–28], and although the vast majority of results concern single-particle problems, e.g., lattice generator schemes [29–36]—flatbands are progressively entering the realm of quantum many-body physics. Even more importantly, a plethora of experimental studies using an impressive variety of physical platforms were performed, which demonstrate the broad applicability of the fine-tuning procedure [27]. Recently many-particles CLS [37–39] and flatband-induced quantum scars [40–42] have been introduced. Networks, which completely lack single-particle dispersion (all bands flat), can completely suppress charge transport with fine-tuned interaction [43–45], while adding on-site disorder and interactions leads to conventional MBL features [46]. We show that disorder free MBL needs just one flatband and at least one dispersive band when accompanied with a proper interaction fine-tuning. Our results explain recent reports on MBL-like dynamics for interacting spinless fermions in particular flatband lattices [47].

Setup — We consider a translationally invariant many-body Hamiltonian

$$\hat{H} = \hat{H}_{\text{sp}} + V\hat{H}_{\text{int}}, \quad \hat{H}_{\text{sp}} = \sum_l \hat{f}_l, \quad \hat{H}_{\text{int}} = \sum_m \hat{g}_m \quad (1)$$

with single-particle \hat{H}_{sp} and interaction \hat{H}_{int} parts written as sums of local operators \hat{f}_l and \hat{g}_m . The integers l, m label unit cells (with either same or different unit cell choices). Each unit cell contains ν sites, and the spectrum of \hat{H}_{sp} ν single-particle bands. The local operators \hat{f}_l, \hat{g}_m are given by products of annihilation and creation operators $\hat{c}_{l,a}, \hat{c}_{l,a}^\dagger$ with $1 \leq a \leq \nu$.

We consider \hat{H}_{sp} , which hosts a flat band E_{FB} while the remaining $\nu - 1$ bands are dispersive. Our results generalize to the case of multiple flatbands. Flatbands with short-range

Published by the American Physical Society under the terms of the [Creative Commons Attribution 4.0 International](https://creativecommons.org/licenses/by/4.0/) license. Further distribution of this work must maintain attribution to the author(s) and the published article's title, journal citation, and DOI. Open access publication funded by the Max Planck Society.

hopping have compact localized states (CLS), and we consider the case where these eigenstates form an orthonormal basis. Following Ref. [29], the original basis $\hat{c}_{l,a}, \hat{c}_{l,a}^\dagger$ of $\hat{\mathcal{H}}_{\text{sp}}$ can be recast via local unitary transformations into a new representation $\hat{a}_{l,a}, \hat{a}_{l,a}^\dagger$ in which $\hat{\mathcal{H}}_{\text{sp}}$ turns into a sum of two commuting components $\hat{\mathcal{H}}_{\text{sp}} = \hat{\mathcal{H}}_{\text{sp}}^f + \hat{\mathcal{H}}_{\text{sp}}^d$. In particular, these components are defined over two disjoint sublattices \mathcal{F} and \mathcal{D} formed by the a single-particle flatband and the $\nu - 1$ dispersive bands respectively. In this *detangled representation*, the flatband component $\hat{\mathcal{H}}_{\text{sp}}^f$ in terms of local operators over sublattice \mathcal{F} reads

$$\hat{\mathcal{H}}_{\text{sp}}^f = E_{\text{FB}} \sum_l \hat{a}_{l,1}^\dagger \hat{a}_{l,1}. \quad (2)$$

The dispersive component $\hat{\mathcal{H}}_{\text{sp}}^d$ is expressed in the Bloch basis $\hat{a}_{l,a}^{(\dagger)} = \sum_{\mathbf{k}} e^{(-)ikl} \hat{a}_{\mathbf{k},a}^{(\dagger)}$ for the annihilation (creation) operators $\hat{a}_{l,a}$ ($\hat{a}_{l,a}^\dagger$) for $2 \leq a \leq \nu$ in terms of local operators over sublattice \mathcal{D}

$$\hat{\mathcal{H}}_{\text{sp}}^d = \sum_{a=2}^{\nu} \sum_{\mathbf{k}} E_a(\mathbf{k}) \hat{a}_{\mathbf{k},a}^\dagger \hat{a}_{\mathbf{k},a} \quad (3)$$

where $\{E_a(\mathbf{k})\}_{a=2}^{\nu}$ are the dispersive bands of $\hat{\mathcal{H}}_{\text{sp}}$.

We assume the interaction $\hat{\mathcal{H}}_{\text{int}}$ in Eq. (1) to be two-body, hence, the local operators \hat{g}_m are written as

$$\hat{g}_m = \sum_{\alpha, \beta, \gamma, \delta=1}^{\nu} J_{\alpha\beta\gamma\delta} \hat{c}_{m,\alpha}^\dagger \hat{c}_{m,\beta}^\dagger \hat{c}_{m,\gamma} \hat{c}_{m,\delta} + \text{H.c.} \quad (4)$$

In the detangled representation of $\hat{\mathcal{H}}_{\text{sp}}$, the interaction $\hat{\mathcal{H}}_{\text{int}}$ splits in three components

$$\hat{\mathcal{H}}_{\text{int}} = \hat{\mathcal{H}}_{\text{int}}^f + \hat{\mathcal{H}}_{\text{int}}^d + \hat{\mathcal{H}}_{\text{int}}^{\text{df}} \quad (5)$$

where (i) the *flatband component* $\hat{\mathcal{H}}_{\text{int}}^f$ is defined over sublattice \mathcal{F} with indices $\alpha, \beta, \gamma, \delta = 1$ in (4); (ii) the *dispersive component* $\hat{\mathcal{H}}_{\text{int}}^d$ is defined over sublattice \mathcal{D} with $2 \leq \alpha, \beta, \gamma, \delta \leq \nu$ in (4); and (iii) the *intra flat-dispersive component* $\hat{\mathcal{H}}_{\text{int}}^{\text{df}}$ is defined by all those terms in Eq. (4), which are not accounted for by either $\hat{\mathcal{H}}_{\text{int}}^f, \hat{\mathcal{H}}_{\text{int}}^d$.

The Hamiltonian $\hat{\mathcal{H}}_{\text{sp}}^f$ in Eq. (2) is formed only by particle number operators $\hat{n} = \hat{a}^\dagger \hat{a}$ and coined *fully detangled* (FD), as introduced in Ref. [43]. Likewise, if we assume the coefficients $J_{\alpha\beta\gamma\delta} = J_{\alpha\beta} \delta_{\alpha,\gamma} \delta_{\beta,\delta}$ in one of the three components $\hat{\mathcal{H}}_{\text{int}}^f, \hat{\mathcal{H}}_{\text{int}}^d, \hat{\mathcal{H}}_{\text{int}}^{\text{df}}$ in Eq. (5) for the correspondent subset of indices, then that component is called FD—as a combination of density operators \hat{n} only.

We first consider Hamiltonians $\hat{\mathcal{H}}$ in Eq. (1) expressed in the detangled basis of $\hat{\mathcal{H}}_{\text{sp}}$ and with $\hat{\mathcal{H}}_{\text{int}}^f, \hat{\mathcal{H}}_{\text{int}}^{\text{df}}$ in Eq. (5) set as fully detangled. This condition forbids particles to move within sublattice \mathcal{F} nor to move from sublattice \mathcal{F} to \mathcal{D} and vice versa. Therefore particles are locked within the flatband component \mathcal{F} and $\hat{\mathcal{H}}$ possesses an extensive set of local conserved quantities $\hat{q}_l = \hat{n}_l = \hat{a}_l^\dagger \hat{a}_l$ for any l . These quantities are simply the occupation numbers of the particles locked in the flatband CLS. Consequently, the relevant Hamiltonian $\hat{\mathcal{H}}$ in Eq. (1) can be reduced to $\hat{\mathcal{H}} = \hat{\mathcal{H}}^{\text{q}} + \hat{\mathcal{H}}_{\text{sp}}^f + V \hat{\mathcal{H}}_{\text{int}}^f$. Indeed, the components $\hat{\mathcal{H}}_{\text{sp}}^f, \hat{\mathcal{H}}_{\text{int}}^f$ depend solely on the conserved quantities $\{\hat{q}_l\}$ and are therefore irrelevant for the particle

dynamics (on sublattice \mathcal{D}). The relevant Hamiltonian

$$\hat{\mathcal{H}}^{\text{q}} = \hat{\mathcal{H}}_{\text{sp}}^d + V \hat{\mathcal{H}}_{\text{int}}^d + \sum_{m,\beta} \hat{\varepsilon}_{m,\beta} \hat{n}_{m,\beta} \quad (6)$$

where $\hat{\varepsilon}_{m,\beta} = V J_{1\beta} \hat{q}_m$ governs the dynamics of interacting particles in the sublattice \mathcal{D} . The term $\hat{\varepsilon}_{m,\beta}$ originates from interaction between the particles in the flat and dispersive bands—i.e., the intra flat-dispersive interaction component $\hat{\mathcal{H}}_{\text{int}}^{\text{df}}$ —and consequently it depends on the values of the conserved quantities $\{\hat{q}_l\}$. Hence, the particles locked in the flatband component act as scatterers for the moving particles in the dispersive component, inducing an effective disordered discrete potential $\hat{\varepsilon}_{m,\beta}$ whose strength is controlled by the interaction strength V . Different realizations of $\hat{\varepsilon}_{m,\beta}$ are generated by different initial conditions, e.g., the distribution of the particles locked in CLS of the flatband component \mathcal{F} .

The Hilbert space of the *full* Hamiltonian $\hat{\mathcal{H}}$ in Eq. (1) is fragmented: It contains irreducible sectors for any filling fraction δ , which are characterized by the the values of the conserved quantities $\{q_l = \langle \psi | \hat{q}_l | \psi \rangle\}$ —similarly to, e.g., Refs. [17–22]. In a given sector, the wave function decomposes as $|\psi\rangle = |\psi_f\rangle \otimes |\psi_d\rangle$, where $|\psi_f\rangle = |q_1, \dots, q_L\rangle$ represents $M_f = \sum_{l \leq L} q_l$ particles locked in the flatband component—i.e., in the CLS—with correspondent flatband filling fraction $\delta_f = M_f/L$. Meanwhile, the second vector $|\psi_d\rangle$ accounts for the remaining mobile particles evolving in the dispersive component whose dynamics is governed by $\hat{\mathcal{H}}^{\text{q}}$ (6) with associated filling fraction δ_d . Both filling fractions δ_f and δ_d result in the overall filling fraction $\delta = \frac{1}{\nu} \delta_f + \frac{\nu-1}{\nu} \delta_d$. The total number T_f of sectors depends on both δ_f , the system size L , and the many-body statistics, e.g., for spinless fermions, $T_f = \binom{L}{M_f}$, while for bosons $T_f = M_f^L$. Indeed, for spinless fermions $q_l = 0, 1$ while for bosons $0 \leq q_l \leq M_f$, which consequently yield in these cases different value ranges for the potential $\hat{\varepsilon}_{m,\beta}$ in Eq. (6) (i.e., different potential strengths).

For a fixed pair of values (δ_f, δ_d) , the flatband filling factor δ_f defines statistical properties of the effective potential $\hat{\varepsilon}_{m,\beta}$ in (6), and consequently the behavior and the properties of the mobile interacting particles in the dispersive component. The interaction V and the two filling fractions δ_f, δ_d are the three control parameters, which can drastically change the transport properties of the considered system. In particular, varying V and δ_d can lead to strong correlations, while varying V and δ_f will control the strength of effective disorder. We therefore expect MBL-like properties, despite the fact that the overall system is translationally invariant. Our considerations apply to systems with any number of single-particle bands ν , in any spatial dimension, and are not restricted to specific types of many-body statistics. Finally we notice that once the mapping is done, our model is no different from the more conventional models with discrete disorder. In particular we expect that disorder realisations are overwhelmingly dominated by typical configurations with similar properties, while atypical disorder realisations—ordered, etc—have no noticeable contribution to the properties of the model.

Signatures of many-body localization transition — As an example we consider spinless fermions in a one-dimensional network with two sites per unit cell, $\nu = 2$. The Hamiltonian

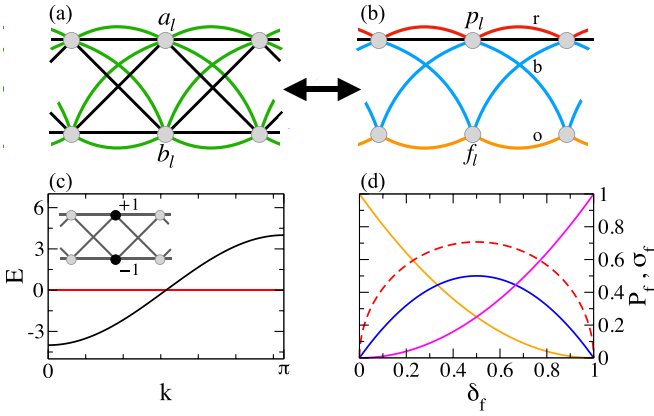


FIG. 1. (a) The network [(7) and (8)] with $\hat{\mathcal{H}}_{\text{sp}}$ (straight black) and $\hat{\mathcal{H}}_{\text{int}}$ (curved green). (b) Detangled $\hat{\mathcal{H}}$ network with $\hat{\mathcal{H}}_{\text{sp}}$ (straight black), $\hat{\mathcal{H}}_{\text{int}}^{\text{d}}$ [curved red (r)], $\hat{\mathcal{H}}_{\text{int}}^{\text{f}}$ [curved blue (b)] and $\hat{\mathcal{H}}_{\text{int}}^{\text{f}}$ [curved orange (o)]. (c) Band structure of $\hat{\mathcal{H}}_{\text{sp}}$ (7), with the inset indicating the nonzero amplitude locations of an $E = 0$ FB CLS (black-filled circles). (d) Probabilities $P_f(\varepsilon_l = 0)$ (orange), $P_f(\varepsilon_l = V)$ (blue), $P_f(\varepsilon_l = 2V)$ (magenta), and standard deviation σ_f (red dashed) of ε_l in Eq. (10) for $V = 1$ vs δ_f .

$\hat{\mathcal{H}} = \hat{\mathcal{H}}_{\text{sp}} + V\hat{\mathcal{H}}_{\text{int}}$ reads

$$\hat{\mathcal{H}}_{\text{sp}} = \sum_l -[(\hat{a}_l^\dagger + \hat{b}_l^\dagger)(\hat{a}_{l+1} + \hat{b}_{l+1}) + \text{H.c.}], \quad (7)$$

$$\hat{\mathcal{H}}_{\text{int}} = \sum_l [\hat{n}_{a,l} + \hat{n}_{b,l}][\hat{n}_{a,l+1} + \hat{n}_{b,l+1}]. \quad (8)$$

The actions of $\hat{\mathcal{H}}_{\text{sp}}$ and $\hat{\mathcal{H}}_{\text{int}}$ are shown in Fig. 1(a) in black-straight lines and green curves respectively. Both single-particle hoppings and interactions connect all sites in neighboring unit cells. Nevertheless the single-particle spectrum of $\hat{\mathcal{H}}_{\text{sp}}$ consists of one dispersive band $E(\mathbf{k}) = -4 \cos(\mathbf{k})$ and one flatband $E_{\text{FB}} = 0$ with its orthonormal CLS shown in Fig. 1(c).

The local unitary transformation $\hat{a}_l = (\hat{p}_l + \hat{f}_l)/\sqrt{2}$ and $\hat{b}_l = (\hat{p}_l - \hat{f}_l)/\sqrt{2}$ introduced in Ref. [29] recasts the Hamiltonian $\hat{\mathcal{H}}_{\text{sp}}$ (7) as $\hat{\mathcal{H}}_{\text{sp}} = \hat{\mathcal{H}}_{\text{sp}}^{\text{f}} + \hat{\mathcal{H}}_{\text{sp}}^{\text{d}}$, where the dispersive part reads $\hat{\mathcal{H}}_{\text{sp}}^{\text{d}} = -2 \sum_l [\hat{p}_l^\dagger \hat{p}_{l+1} + \text{H.c.}]$, while the flatband component $\hat{\mathcal{H}}_{\text{sp}}^{\text{f}} = 0$. The dispersive component $\hat{\mathcal{H}}_{\text{sp}}^{\text{d}}$ is shown in Fig. 1(b) with black horizontal line. On the other hand, the interaction $\hat{\mathcal{H}}_{\text{int}}$ (8) is invariant under the unitary rotation. In the detangled basis (p_l, f_l) , the interaction $\hat{\mathcal{H}}_{\text{int}}$ breaks down into three components (5): $\hat{\mathcal{H}}_{\text{int}}^{\text{f}} = \sum_l \hat{n}_{p,l} \hat{n}_{f,l+1}$, $\hat{\mathcal{H}}_{\text{int}}^{\text{d}} = \sum_l \hat{n}_{p,l} \hat{n}_{p,l+1}$, and $\hat{\mathcal{H}}_{\text{int}}^{\text{df}} = \sum_l [\hat{n}_{p,l} \hat{n}_{f,l+1} + \hat{n}_{f,l} \hat{n}_{p,l+1}]$, which are shown in Fig. 1(b) with orange, red, and blue curves respectively.

The relevant Hamiltonian $\hat{\mathcal{H}}^{\text{q}}$ (6) governing the dynamics of the particles evolving in the dispersive component reads

$$\hat{\mathcal{H}}^{\text{q}} = \sum_l [\varepsilon_l \hat{n}_{p,l} - 2(\hat{p}_l^\dagger \hat{p}_{l+1} + \text{H.c.}) + V \hat{n}_{p,l} \hat{n}_{p,l+1}], \quad (9)$$

$$\varepsilon_l = V(\hat{q}_{l+1} + \hat{q}_{l-1}), \quad (10)$$

with $\hat{n}_{p,l} = \hat{p}_l^\dagger \hat{p}_l$. The conserved quantities $\hat{q}_l = \hat{f}_l^\dagger \hat{f}_l$ take the values $\{0, 1\}$ —i.e., each \hat{q}_l accounts for the presence/absence of a spinless fermion locked at the l th flatband CLS f_l . The

potential ε_l (10) follows from the intra flat-dispersive interaction component $\hat{\mathcal{H}}_{\text{int}}^{\text{df}}$, which represent the interaction between the mobile particles with those locked in the flatband CLS. In other words, $\hat{\mathcal{H}}^{\text{q}}$ (9) describes interacting spinless fermions in a one-dimensional chain with a random ternary potential $\varepsilon_l \in \{0, V, 2V\}$ induced by the extensive set of conserved quantities \hat{q}_l . Ternary disorder with equal probabilities $1/3$ has been studied in Ref. [48] where an MBL transition was reported for the Heisenberg spin-1/2 chain by varying the strength of interaction and interaction strengths are tuned by the same control parameter V in Eq. (9). Further, the probabilities of $\varepsilon_l = \{0, V, 2V\}$ depend on the filling fraction δ_f of the flatband component. Indeed, at a given site f_l the probability that $\hat{q}_l = 0$ is $1 - \delta_f$, while the probability that $\hat{q}_l = 1$ is δ_f . Consequently, as $\varepsilon_l = 0$ occurs when both $\hat{q}_{l\pm 1} = 0$, then $P_f(\varepsilon_l = 0) = (1 - \delta_f)^2$. Analogously follows that $P_f(\varepsilon_l = 2V) = \delta_f^2$, while $P_f(\varepsilon_l = V) = 2\delta_f(1 - \delta_f)$. These three curves are shown in Fig. 1(d) in solid lines, where we also include in dashed line the standard deviation $\sigma_f = V\sqrt{2\delta_f(1 - \delta_f)}$ of ε_l from the average potential $\langle \varepsilon_l \rangle_l = 2V\delta_f$ [49]. Note as well that equal probabilities $1/3$ are never realized for any filling fraction value.

We identify the transition between ergodic (thermalized, metallic, delocalized) and nonergodic (nonthermalized, insulating, localized) regimes of our system by analyzing the energy-resolved adjacent gap ratio $r^{(n)} = \min(s^{(n)}, s^{(n+1)}) / \max(s^{(n)}, s^{(n+1)})$ with $s^{(n)} = E_n - E_{n-1}$ for the eigenenergies E_n [50]. The expectation is that the ergodic regime corresponds to the Gaussian orthogonal ensemble (GOE) with $r_{\text{GOE}} = 0.5307$ [51]. At variance, the nonergodic regime should yield a Poisson distribution of level spacings with $r_{\text{Poisson}} \approx 0.3863$.

We diagonalize $\hat{\mathcal{H}}^{\text{q}}$ in Eq. (9) for $L = 16$ sites with open boundary conditions averaging over 200 realizations at fixed filling fractions δ_f and δ_d —i.e., over 200 sectors of the Hilbert space [52]. Following Ref. [53], the spectrum is normalized as $\epsilon(E_n) = (E_n - E_{\text{min}}) / (E_{\text{max}} - E_{\text{min}})$ for each realization, divided into 50 intervals, and the mean adjacent gap ratio $\langle r \rangle$ is computed for each segment separately. The results are reported in Figs. 2(a)–2(d). In all cases, the MBL transition emerges at large enough interaction strength $V \gg 1$. Note that the MBL transition occurs for different values of V within different irreducible sectors of the Hilbert space characterized by different pairs of filling fractions (δ_f, δ_d) despite sharing the same global filling δ —e.g., Figs. 2(b) and 2(c).

Our construction also explains the nonergodic dynamics observed for a $\nu = 3$ case with spinless fermions in Ref. [47]. The model is shown in Fig. 3(a) and it is described by the Hamiltonian $\hat{\mathcal{H}} = \hat{\mathcal{H}}_{\text{sp}} + V\hat{\mathcal{H}}_{\text{int}}$ with

$$\hat{\mathcal{H}}_{\text{sp}} = - \sum_l [(\hat{a}_l^\dagger + \hat{b}_l^\dagger)(\hat{c}_l + \hat{c}_{l+1}) + \text{H.c.}], \quad (11)$$

$$\hat{\mathcal{H}}_{\text{int}} = \sum_l [\hat{n}_{a,l} + \hat{n}_{b,l}][\hat{n}_{c,l} + \hat{n}_{c,l+1}] + \hat{n}_{a,l} \hat{n}_{b,l}. \quad (12)$$

The single-particle spectrum of $\hat{\mathcal{H}}_{\text{sp}}$ consists of two dispersive bands $E_{1,2}(\mathbf{k}) = \pm 2\sqrt{2} \cos(\mathbf{k}/2)$ and a flatband $E = 0$ with orthonormal CLS. Detangling local unitary transformations for the single-particle Hamiltonian have been reported in Ref.

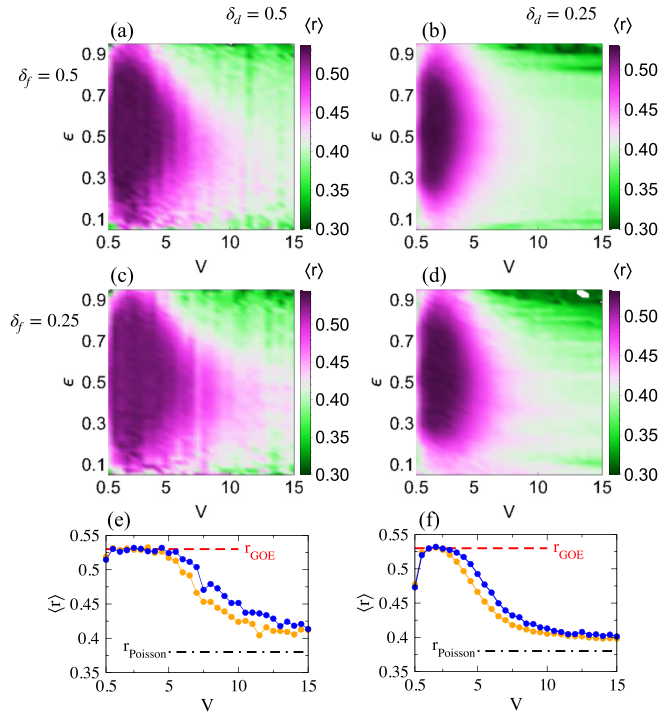


FIG. 2. [(a)–(d)] Energy resolved mean adjacent gap ratio $\langle r \rangle$ vs (ϵ, V) for model (9) and (10). (a) $\delta_d = 0.5$; $\delta_f = 0.5$; (b) $\delta_d = 0.25$; $\delta_f = 0.5$; (c) $\delta_d = 0.5$; $\delta_f = 0.25$; (d) $\delta_d = 0.25$; $\delta_f = 0.25$. (e) $\langle r \rangle$ vs V for $\epsilon = 0.5$ at $\delta_f = 0.5$ (orange) and $\delta_f = 0.25$ (blue) for $\delta_d = 0.5$. (f) Same as (e) for $\delta_d = 0.25$. The system size $L = 16$ for all cases.

[29]. For spinless fermions, the resulting system is shown in Fig. 3(b). In the new basis the product terms in Eq. (12) decompose into $\hat{\mathcal{H}}_{\text{int}}^f = 0$, $\hat{\mathcal{H}}_{\text{int}}^d = \sum_l \hat{n}_{p,l}(\hat{n}_{c,l} + \hat{n}_{c,l+1})$, and $\hat{\mathcal{H}}_{\text{int}}^{\text{df}} = \sum_l \hat{n}_{f,l}(\hat{n}_{c,l} + \hat{n}_{c,l+1})$ —defining the Hamiltonian

$$\hat{\mathcal{H}}^q = \sum_l [\hat{\epsilon}_l \hat{n}_{c,l} - \sqrt{2}(\hat{p}_l^\dagger \hat{c}_l + \hat{p}_l \hat{c}_{l+1} + \text{H.c.}) + V \hat{n}_{p,l}(\hat{n}_{c,l} + \hat{n}_{c,l+1})] \quad (13)$$

with the potential $\hat{\epsilon}_l = V(\hat{q}_{l-1} + \hat{q}_l)$. Interestingly, the terms $\hat{n}_{a,l} \hat{n}_{b,l}$ result in $\hat{p}_l^\dagger \hat{p}_l^\dagger \hat{f}_l \hat{f}_l + \text{H.c.}$ in addition to the Hubbard interaction terms on p, f sites, which could violate the fine-tuning. These terms need more than one particle per state and therefore disappear for spinless fermions. Consequently they do not enter $\hat{\mathcal{H}}^q$ in Eq. (13). However such terms will appear for example bosons and spinful fermions, and will move pairs of particles between sublattices \mathcal{F} to \mathcal{D} . Consequently the quantities \hat{q}_l will be no longer conserved for spinful fermions or bosons, and will wash out the irreducible sectors in the Hilbert space of $\hat{\mathcal{H}}$. In Figs. 3(c) and 3(d) we plot the energy-resolved mean adjacent gap ratio $\langle r \rangle$ for two pairs of filling factors δ_d and δ_f upon increasing the interaction strength V . We observe signatures of an MBL transition for large $V \gg 1$. The transition is further visualized in Fig. 3(e) where we plot the energy-resolved $\langle r \rangle$ versus V around $\epsilon = 0.5$.

Conclusions — To conclude, we showed that disorder free many body localization is obtained for flatband networks with fine-tuned interaction. The flatband supports compact localized states, and the fine-tuning locks particles in these states

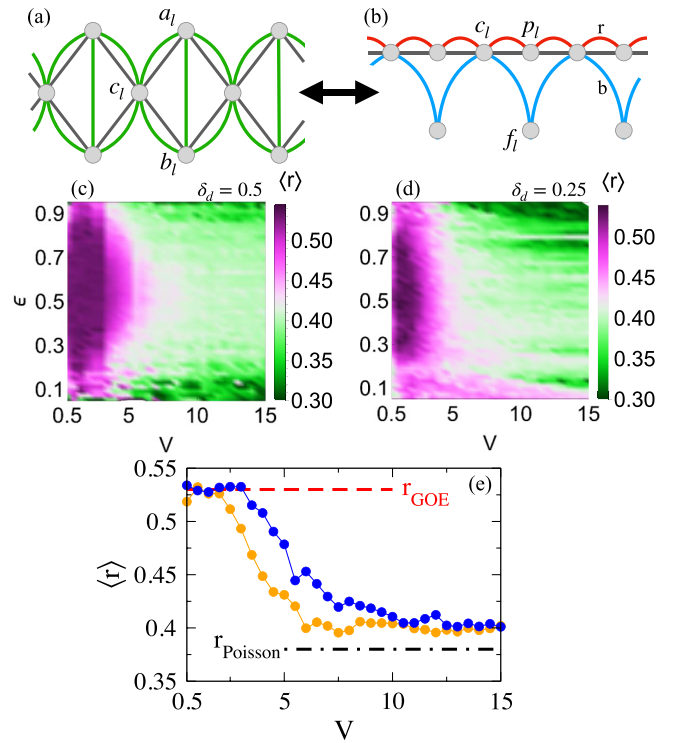


FIG. 3. (a) The network [(11) and (12)] with $\hat{\mathcal{H}}_{\text{sp}}$ (straight black) and $\hat{\mathcal{H}}_{\text{int}}$ (curved green). (b) Detangled network (13) with $\hat{\mathcal{H}}_{\text{int}}^d$ [red (r)] and $\hat{\mathcal{H}}_{\text{int}}^{\text{df}}$ [blue (b)]. [(c)–(d)] Energy resolved mean adjacent gap ratio $\langle r \rangle$ versus (ϵ, V) for (c) $\delta_d = 0.5$; $\delta_f = 0.5$; (d) $\delta_d = 0.25$; $\delta_f = 0.5$. (e) $\langle r \rangle$ vs V around $\epsilon = 0.5$ at $\delta_d = 0.5$ (blue) and $\delta_d = 0.25$ (orange) for $\delta_f = 0.25$. The system size $L = 16$ for all cases.

even in the presence of interaction. These locked particles turn into scatterers for particles from dispersive states. These families have been obtained by fine-tuning two-body interaction terms on single-particle lattices that host dispersive bands and flatbands with orthonormal sets of CLS. We showed that these scatterers are equivalent to conserved quantities and enter the Hamiltonian of the system inducing an effective disorder. We studied numerically two sample cases, Eqs. (7), (8) and Eqs. (11), (12), for spinless fermions in 1D, confirming that such disorder indeed induces signatures of many-body localization transition upon changing the interaction strength. We performed the simulations for a single size $L = 16$ for the two examples considered. For generic models featuring MBL one usually has to consider several system sizes and perform finite size scaling to confirm the transition. We note that the system sizes available for exact or even sparse diagonalisation might not be enough to confirm the presence of the MBL transition [54]. In our case, however, the effective models (6) are essentially the standard models studied in the MBL community, but with two differences: (i) the disorder is discrete—this is not relevant, as shown in Ref. [48]; (ii) the interaction and the disorder scale with the same interaction strength parameter V . This suggests that the signatures of the MBL transition are to be expected, based on all the previous studies of such models. However (ii) makes our models only explore a single line on the phase diagram of a typical MBL model, potentially allowing to avoid crossing the phase boundary. Under this

condition, i.e., mapping to the standard MBL model, it is justified to consider a single system size: A single size is enough for us to check whether the variation of the parameter V , allows to cross the phase boundary to the possible MBL phase. The finite-size scaling in our model would then be similar to the conventional MBL models if the crossing is present.

The proposed fine-tuning scheme applies in any lattice dimensions and for any type of many-body statistics. We therefore arrive at a systematic generic generator of quantum many-body systems characterized by an extensive number of local conserved operators, which result in ergodicity breaking phenomena. Another important extension is that we can abandon the translational invariance of \hat{H} and consider local rotations and/or the energies E_a in Eq. (2) unit cell dependent; one can also consider flatband Hamiltonians \hat{H}_{sp} without orthonormal sets of CLS [55].

Our findings explain recent spinless fermion results for a rhombic lattice considered by Daumann *et al.* [47] (orthonormal set of CLS) and hint those for a sawtooth ladder considered by Khare *et al.* [56] (nonorthonormal set of CLS). It is straightforward to observe that for total filling fraction $\delta \leq 1/\nu$ there are exact eigenstates with all particles

confined to single-particle CLS. These eigenstates coexist with extended eigenstates characterized by volume-law entanglement, and become flatband many-body quantum scars [39–42]. Many-body quantum scars are related to weak ergodicity breaking phenomena [57–59].

The above obtained fine-tuned models can be both appealing from a purely mathematical point of view, and for experimentally relevant setups. Indeed, flatband networks have been indeed experimentally realized in diverse platforms, such as ultracold atoms [60] and photonic lattices [61–63]—see also [26–28]. Flatband systems with orthonormal CLS allow the energy levels E_{FB} in Eq. (2) to be freely tuned. They can thus either cross the dispersive bands $E_a(\mathbf{k})$ in Eq. (3) or be gapped away from dispersive bands. This freedom allows to tune the flatband energy at the Fermi level, and to load the particles into the flatband states prior reaching the complete filling of dispersive bands in an experimentally achievable way.

This work was supported by the Institute for Basic Science (Project No. IBS-R024-D1). We thank I. Khaymovich for helpful discussions.

-
- [1] P. W. Anderson, Absence of diffusion in certain random lattices, *Phys. Rev.* **109**, 1492 (1958).
- [2] L. Fleishman and P. W. Anderson, Interactions and the Anderson transition, *Phys. Rev. B* **21**, 2366 (1980).
- [3] B. L. Altshuler, Y. Gefen, A. Kamenev, and L. S. Levitov, Quasiparticle Lifetime in a Finite System: A Nonperturbative Approach, *Phys. Rev. Lett.* **78**, 2803 (1997).
- [4] P. Jacquod and D. L. Shepelyansky, Emergence of Quantum Chaos in Finite Interacting Fermi Systems, *Phys. Rev. Lett.* **79**, 1837 (1997).
- [5] I. V. Gornyi, A. D. Mirlin, and D. G. Polyakov, Interacting Electrons in Disordered Wires: Anderson Localization and Low- t Transport, *Phys. Rev. Lett.* **95**, 206603 (2005).
- [6] D. M. Basko, I. L. Aleiner, and B. L. Altshuler, Metal–insulator transition in a weakly interacting many-electron system with localized single-particle states, *Ann. Phys. (NY)* **321**, 1126 (2006).
- [7] D. A. Abanin and Z. Papić, Recent progress in many-body localization, *Ann. Phys. (NY)* **529**, 1700169 (2017).
- [8] D. A. Abanin, E. Altman, I. Bloch, and M. Serbyn, Colloquium: Many-body localization, thermalization, and entanglement, *Rev. Mod. Phys.* **91**, 021001 (2019).
- [9] M. Schiulaz, A. Silva, and M. Müller, Dynamics in many-body localized quantum systems without disorder, *Phys. Rev. B* **91**, 184202 (2015).
- [10] M. van Horssen, E. Levi, and J. P. Garrahan, Dynamics of many-body localization in a translation-invariant quantum glass model, *Phys. Rev. B* **92**, 100305(R) (2015).
- [11] J. M. Hickey, S. Genway, and J. P. Garrahan, Signatures of many-body localisation in a system without disorder and the relation to a glass transition, *J. Stat. Mech.: Theory Exp.* (2016) 054047.
- [12] R. Mondaini and Z. Cai, Many-body self-localization in a translation-invariant Hamiltonian, *Phys. Rev. B* **96**, 035153 (2017).
- [13] M. Pino, L. B. Ioffe, and B. L. Altshuler, Nonergodic metallic and insulating phases of Josephson junction chains, *Proc. Natl. Acad. Sci. USA* **113**, 536 (2016).
- [14] M. Schulz, C. A. Hooley, R. Moessner, and F. Pollmann, Stark Many-Body Localization, *Phys. Rev. Lett.* **122**, 040606 (2019).
- [15] E. van Nieuwenburg, Y. Baum, and G. Refael, From Bloch oscillations to many-body localization in clean interacting systems, *Proc. Natl. Acad. Sci. USA* **116**, 9269 (2019).
- [16] E. V. H. Doggen, I. V. Gornyi, and D. G. Polyakov, Stark many-body localization: Evidence for Hilbert-space shattering, *Phys. Rev. B* **103**, L100202 (2021).
- [17] A. Smith, J. Knolle, D. L. Kovrizhin, and R. Moessner, Disorder-Free Localization, *Phys. Rev. Lett.* **118**, 266601 (2017).
- [18] A. Smith, J. Knolle, R. Moessner, and D. L. Kovrizhin, Absence of Ergodicity without Quenched Disorder: From Quantum Disentangled Liquids to Many-Body Localization, *Phys. Rev. Lett.* **119**, 176601 (2017).
- [19] A. Smith, J. Knolle, R. Moessner, and D. L. Kovrizhin, Dynamical localization in z_2 lattice gauge theories, *Phys. Rev. B* **97**, 245137 (2018).
- [20] M. Brenes, M. Dalmonte, M. Heyl, and A. Scardicchio, Many-Body Localization Dynamics from Gauge Invariance, *Phys. Rev. Lett.* **120**, 030601 (2018).
- [21] P. Karpov, R. Verdel, Y.-P. Huang, M. Schmitt, and M. Heyl, Disorder-Free Localization in an Interacting 2D Lattice Gauge Theory, *Phys. Rev. Lett.* **126**, 130401 (2021).
- [22] O. Hart, S. Gopalakrishnan, and C. Castelnovo, Logarithmic Entanglement Growth from Disorder-Free Localization in

- the Two-Leg Compass Ladder, *Phys. Rev. Lett.* **126**, 227202 (2021).
- [23] P. Sala, T. Rakovszky, R. Verresen, M. Knap, and F. Pollmann, Ergodicity Breaking Arising from Hilbert Space Fragmentation in Dipole-Conserving Hamiltonians, *Phys. Rev. X* **10**, 011047 (2020).
- [24] Z.-C. Yang, F. Liu, A. V. Gorshkov, and T. Iadecola, Hilbert Space Fragmentation from Strict Confinement, *Phys. Rev. Lett.* **124**, 207602 (2020).
- [25] S. Scherg, T. Kohlert, P. Sala, F. Pollmann, B. H. M., I. Bloch, and M. Aidelsburger, Observing non-ergodicity due to kinetic constraints in tilted fermi-hubbard chains, *Nat Commun* **12**, 4490 (2021).
- [26] O. Derzhko, J. Richter, and M. Maksymenko, Strongly correlated flat-band systems: The route from Heisenberg spins to Hubbard electrons, *Int. J. Mod. Phys. B* **29**, 1530007 (2015).
- [27] D. Leykam, A. Andreanov, and S. Flach, Artificial flat band systems: From lattice models to experiments, *Adv. Phys.: X* **3**, 1473052 (2018).
- [28] D. Leykam and S. Flach, Perspective: Photonic flatbands, *APL Photonics* **3**, 070901 (2018).
- [29] S. Flach, D. Leykam, J. D. Bodyfelt, P. Matthies, and A. S. Desyatnikov, Detangling flat bands into Fano lattices, *Europhys. Lett.* **105**, 30001 (2014).
- [30] R. G. Dias and J. D. Gouveia, Origami rules for the construction of localized eigenstates of the Hubbard model in decorated lattices, *Sci. Rep.* **5**, 16852 (2015).
- [31] A. Ramachandran, A. Andreanov, and S. Flach, Chiral flat bands: Existence, engineering, and stability, *Phys. Rev. B* **96**, 161104(R) (2017).
- [32] W. Maimaiti, A. Andreanov, H. C. Park, O. Gendelman, and S. Flach, Compact localized states and flat-band generators in one dimension, *Phys. Rev. B* **95**, 115135 (2017).
- [33] M. Röntgen, C. V. Morfonios, and P. Schmelcher, Compact localized states and flat bands from local symmetry partitioning, *Phys. Rev. B* **97**, 035161 (2018).
- [34] L. A. Toikka and A. Andreanov, Necessary and sufficient conditions for flat bands in m-dimensional n-band lattices with complex-valued nearest-neighbour hopping, *J. Phys. A* **52**, 02LT04 (2018).
- [35] W. Maimaiti, S. Flach, and A. Andreanov, Universal $d = 1$ flat band generator from compact localized states, *Phys. Rev. B* **99**, 125129 (2019).
- [36] W. Maimaiti, A. Andreanov, and S. Flach, Flat-band generator in two dimensions, *Phys. Rev. B* **103**, 165116 (2021).
- [37] M. Tovmasyan, S. Peotta, L. Liang, P. Törmä, and S. D. Huber, Preformed pairs in flat bloch bands, *Phys. Rev. B* **98**, 134513 (2018).
- [38] S. Tilleke, M. Daumann, and T. Dahm, Nearest neighbour particle-particle interaction in fermionic quasi one-dimensional flat band lattices, *Z. Naturforsch. A* **75**, 393 (2020).
- [39] C. Danieli, A. Andreanov, T. Mithun, and S. Flach, Quantum caging in interacting many-body all-bands-flat lattices, *Phys. Rev. B* **104**, 085132 (2021).
- [40] O. Hart, G. De Tomasi, and C. Castelnovo, From compact localized states to many-body scars in the random quantum comb, *Phys. Rev. Research* **2**, 043267 (2020).
- [41] P. A. McClarty, M. Haque, A. Sen, and J. Richter, Disorder-free localization and many-body quantum scars from magnetic frustration, *Phys. Rev. B* **102**, 224303 (2020).
- [42] Y. Kuno, T. Mizoguchi, and Y. Hatsugai, Flat band quantum scar, *Phys. Rev. B* **102**, 241115(R) (2020).
- [43] C. Danieli, A. Andreanov, and S. Flach, Many-body flatband localization, *Phys. Rev. B* **102**, 041116(R) (2020).
- [44] Y. Kuno, T. Orito, and I. Ichinose, Flat-band many-body localization and ergodicity breaking in the Creutz ladder, *New J. Phys.* **22**, 013032 (2020).
- [45] T. Orito, Y. Kuno, and I. Ichinose, Exact projector Hamiltonian, local integrals of motion, and many-body localization with symmetry-protected topological order, *Phys. Rev. B* **101**, 224308 (2020).
- [46] N. Roy, A. Ramachandran, and A. Sharma, Interplay of disorder and interactions in a flat-band supporting diamond chain, *Phys. Rev. Research* **2**, 043395 (2020).
- [47] M. Daumann, R. Steinigeweg, and T. Dahm, Many-body localization in translational invariant diamond ladders with flat bands, [arXiv:2009.09705](https://arxiv.org/abs/2009.09705).
- [48] J. Janarek, D. Delande, and J. Zakrzewski, Discrete disorder models for many-body localization, *Phys. Rev. B* **97**, 155133 (2018).
- [49] The first moment (average) of the potential ε_l is $E(\varepsilon_l) = 2V\delta_f$, while its second moment is $E(\varepsilon_l^2) = 2V^2\delta_f(1 + \delta_f)$. The standard deviation $\sigma_f = \sqrt{E(\varepsilon_l^2) - E(\varepsilon_l)^2}$ reads $\sigma_f = V\sqrt{2\delta_f + 2\delta_f^2 + 4\delta_f^3} = V\sqrt{2\delta_f(1 - \delta_f)}$.
- [50] V. Oganesyan and D. A. Huse, Localization of interacting fermions at high temperature, *Phys. Rev. B* **75**, 155111 (2007).
- [51] Y. Y. Atas, E. Bogomolny, O. Giraud, and G. Roux, Distribution of the Ratio of Consecutive Level Spacings in Random Matrix Ensembles, *Phys. Rev. Lett.* **110**, 084101 (2013).
- [52] No changes in the mobility edge profiles appeared while averaging over a different number of realizations. We note however that given a single system size $L = 16$ we cannot make any reliable predictions about the presence of the mobility edge in the thermodynamic limit.
- [53] D. J. Luitz, N. Laflorencie, and F. Alet, Many-body localization edge in the random-field Heisenberg chain, *Phys. Rev. B* **91**, 081103(R) (2015).
- [54] R. K. Panda, A. Scardicchio, M. Schulz, S. R. Taylor, and M. Žnidarič, Can we study the many-body localisation transition? *Europhys. Lett.* **128**, 67003 (2020).
- [55] D. Leykam, J. D. Bodyfelt, A. S. Desyatnikov, and S. Flach, Localization of weakly disordered flat band states, *Eur. Phys. J. B* **90**, 1 (2017).
- [56] R. Khare and S. Choudhury, Localized dynamics following a quantum quench in a non-integrable system: An example on the sawtooth ladder, *J. Phys. B* **54**, 015301 (2020).
- [57] C. J. Turner, A. A. Michailidis, D. A. Abanin, M. Serbyn, and Z. Papić, Weak ergodicity breaking from quantum many-body scars, *Nat. Phys.* **14**, 745 (2018).
- [58] M. Serbyn, D. A. Abanin, and Z. Papić, Quantum many-body scars and weak breaking of ergodicity, *Nat. Phys.* **17**, 675 (2021).
- [59] S. Pilatowsky-Cameo, D. Villaseñor, M. A. Bastarrachea-Magnani, S. Lerma-Hernandez, L. F. Santos, and J. G. Hirsch, Ubiquitous quantum scarring does not prevent ergodicity, *Nat. Commun.* **12**, 852 (2021).

- [60] S. Taie, H. Ozawa, T. Ichinose, T. Nishio, S. Nakajima, and Y. Takahashi, Coherent driving and freezing of bosonic matter wave in an optical lieb lattice, [Sci. Adv. **1**, e1500854 \(2015\)](#).
- [61] S. Mukherjee, A. Spracklen, D. Choudhury, N. Goldman, P. Öhberg, E. Andersson, and R. R. Thomson, Observation of a Localized Flat-Band State in a Photonic Lieb Lattice, [Phys. Rev. Lett. **114**, 245504 \(2015\)](#).
- [62] R. A. Vicencio, C. Cantillano, L. Morales-Inostroza, B. Real, C. Mejía-Cortés, S. Weimann, A. Szameit, and M. I. Molina, Observation of Localized States in Lieb Photonic Lattices, [Phys. Rev. Lett. **114**, 245503 \(2015\)](#).
- [63] S. Weimann, L. Morales-Inostroza, B. Real, C. Cantillano, A. Szameit, and R. A. Vicencio, Transport in sawtooth photonic lattices, [Opt. Lett. **41**, 2414 \(2016\)](#).